CA8406832

AECL-7680

ATOMIC ENERGY OF CANADA LIMITED

L'ÉNERGIE ATOMIQUE DU CANADA LIMITÉE

MONTE AND ANAL1: A GENERAL PURPOSE MONTE CARLO SIMULATION FOR THE DESIGN OF SINGLE-SLICE POSITRON EMISSION TOMOGRAPHY RING CAMERAS

MONTE et ANAL1: Simulation universelle de Monte Carlo pour la conception de caméras tomographiques annulaires émettrices de positrons en simples tranches

L.R. LUPTON and N.A. KELLER

Chalk River Nuclear Laboratories Laboratoires nucléaires de Chalk River

Chalk River, Ontario

September 1982 septembre

ATOMIC ENERGY OF CANADA LIMITED

MONTE AND ANAL1: A GENERAL PURPOSE MONTE CARLO SIMULATION FOR THE DESIGN OF SINGLE-SLICE POSITRON EMISSION TOMOGRAPHY RING CAMERAS

by

L.R. Lupton and N.A. Keller

Instrument Development Branch
Chalk River Nuclear Laboratories
Chalk River, Ontario K0J 1J0

1982 September

AECL-7680

L'ENERGIE ATOMIQUE DU CANADA, LIMITEE

MONTE et ANAL1:
Simulation universelle de Monte Carlo pour la conception de caméras tomographiques annulaires émettrices de positrons en simples tranches

par

L.R. Lupton et N.A. Keller

Résumé

La conception d'une caméra tomographique annulaire émettrice de positrons donne lieu à des compromis entre des facteurs comme la sensibilité, la résolution et le coût. Pour faciliter la conception, on a développé une simulation Monte Carlo pour un type de caméra à simple anneau. Le modèle comprend un fantôme muni d'une source, des collimateurs, des détecteurs et il peut avoir des écrans d'ombre et des diaphragmes inter-cristaux. Les rayons gamma individuels sont suivis dans les matériaux du système jusqu'à ce qu'ils s'échappent, puis ils sont absorbés ou détectés. Les interactions Compton et photoélectriques sont modélisées. Toutes les dimensions du système sont variables dans le calcul. Les données de coïncidence et d'unicité sont enregistrées selon le type (vraies ou diffusées), l'origine d'annihilation et l'énergie détectée. Les flux des photons à divers points d'intérêt, comme le bord du fantôme et le collimateur, sont disponibles.

Ce rapport passe en revue les données fondamentales du tomographe émetteur de positrons, il décrit la physique impliquée dans la simulation et il fournit un aperçu des routines.

Département de développement des instruments
Laboratoires nucléaires de Chalk River
Chalk River, Ontario K0J 1J0

Septembre 1982

AECL-7680

ATOMIC ENERGY OF CANADA LIMITED

MONTE AND ANAL1: A GENERAL PURPOSE MONTE CARLO SIMULATION FOR THE DESIGN OF SINGLE-SLICE POSITRON EMISSION TOMOGRAPHY RING CAMERAS

by

L.R. Lupton and N.A. Keller

ABSTRACT

The design of a positron emission tomography (PET) ring camera involves trade-offs between such things as sensitivity, resolution and cost. As a design aid, a Monte Carlo simulation of a single-ring camera system has been developed. The model includes a source-filled phantom, collimators, detectors, and optional shadow shields and inter-crystal septa. Individual gamma-rays are tracked within the system materials until they escape, are absorbed, or are detected. Compton and photoelectric interactions are modelled. All system dimensions are variable within the computation. Coincidence and singles data are recorded according to type (true or scattered), annihilation origin, and detected energy. Photon fluxes at various points of interest, such as the edge of the phantom and the collimator, are available.

This report reviews the basics of PET, describes the physics involved in the simulation, and provides detailed outlines of the routines.

Instrument Development Branch
Chalk River Nuclear Laboratories
Chalk River, Ontario K0J 1J0

1982 September

AECL-7680

TABLE OF CONTENTS

LIST OF FIGURES

LIST OF TABLES

1. INTRODUCTION

A continuing goal of medicine is the earliest possible observation and identification of abnormal biochemical activity within an organ. With radioactive isotopes, it is possible to administer a tagged substance to a patient and then follow the movement of the compound within the body. One technique for performing such measurements is positron emission tomography (PET). In this procedure, a chemical compound is labelled with a radioactive isotope that decays by emitting a positron. The positron subsequently annihilates with an electron to yield two 511 keV γ-rays that are emitted in nearly opposite directions. The detection of these coincident γ-rays by a pair of detectors external to the patient determines the position of the activity to be along the line joining the detectors, as shown in Figure 1. By using a complete ring of detectors, and recording coincidences between all detector pairs, an arbitrary source distribution can be reconstructed [1]. In the reconstruction, the image area is divided into a 2-D computer memory representation, where the intensity of each picture element, or pixel, represents the average source activity within the pixel boundary. The coincidence lines from the detected photon-pairs are "drawn" or "back-projected" across the image area. Each time they intersect a pixel, the intensity in the pixel is incremented by one. After several million back-projections, an estimate of the activity distribution is achieved. The biochemical activity of the compound onto which the positron emitting source was tagged can be deduced from this distribution.

Unfortunately, as the γ-rays pass through the subject, they interact with it and undergo Compton scatter or photoelectric absorption. Photoelectric absorption is relatively unimportant in body tissue for photons of the energies of interest. Compton scatter is, however, significant because

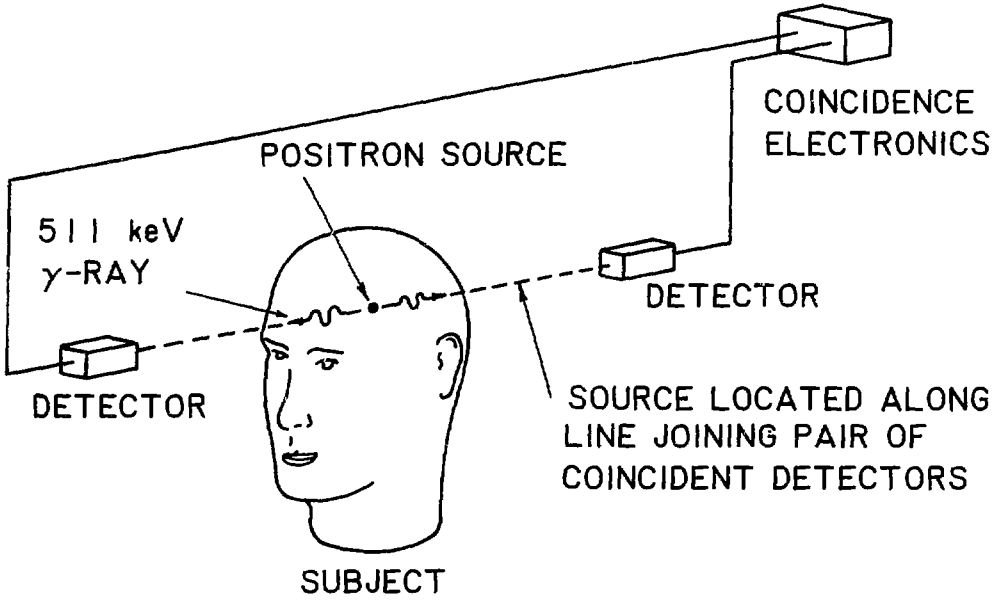

FIGURE 1: THE USE OF COINCIDENCE DETECTION TO LOCATE A POSITRON EMITTING SOURCE

it causes the γ-rays to change direction before detection. This leads to erroneous information as to the source location. Some of the scattered photons can be rejected by energy discrimination since the photon's energy is changed when it Compton scatters. However, a sizeable number of these events are still accepted as the average energy lost is less than the energy resolution of the detectors used. Random coincidences between γ-rays from two different annihilations can also occur. Thus, three types of coincidence events exist in PET, as summarized in Figure 2. Minimizing the detection of scattered and random coincidences while maintaining a high sensitivity for trues events is of primary importance in the design of a PET scanner.

In the design process, several geometric parameters such as patient port size, slice thickness, ring diameter and detector width must be considered. Fundamental to the selection of these parameters are tradeoffs between cost, system sensitivity, and resolution. In addition, the type of research and/or clinical studies for which the camera will be used also has a bearing on the system geometry. Several analytical studies [2-8] of the effect of these parameters have been published. However, during testing of the prototype Therascan 3128 camera, developed by the AECL-Radiochemical Company, it was found that discrepancies existed between the measured camera sensitivity, Compton scatter fraction and random coincidence rate and those predicted using formulae given in these studies. As these formulae had been derived using several simplifying assumptions, it was apparent that a more sophisticated calculation was required to adequately model this camera. This was achieved by simulating the photon transport within the camera by Monte Carlo techniques [9]. The simulation is broad enough in scope that it can be used as a design aid.

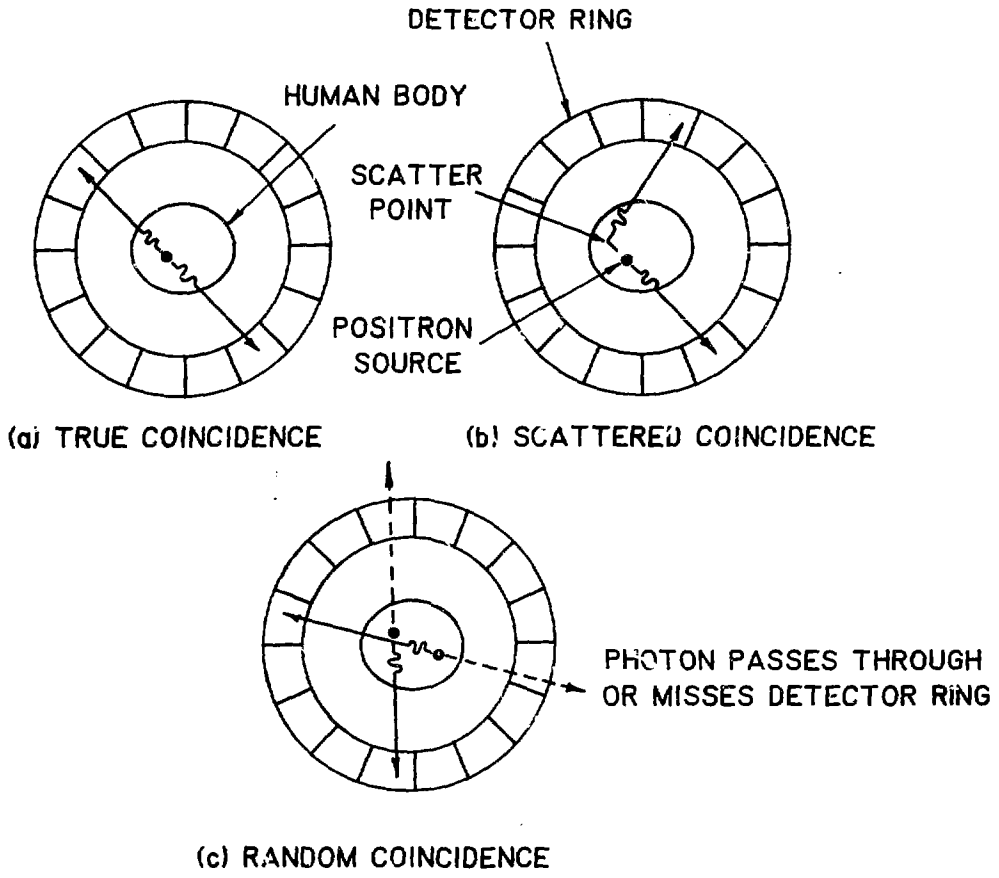

FIGURE 2: THREE TYPES OF COINCIDENCE EVENTS THAT OCCUR IN POSITRON EMISSION TOMOGRAPHY

The simulation package has been written in FORTRAN to run on a CDC CYBER 175 computer. With some modifications, it can be made to run on most mainframe and mini-computers.

This report summarizes the techniques used in the simulation and includes detailed outlines of the program modules and a summary of the analysis provided in the output. Future reports will present analyses of the data obtained from the simulation.

2. SIMULATION PACKAGE

2.1 General Overview

The model of a PET camera used in the simulation is illustrated in Figure 3. Photon transport is modelled in four components, namely a water-filled phantom containing the source, a collimator, shadow-shields or beam blockers, on the face of the detectors, and detectors. These components are discussed below.

To test PET camera systems, phantoms with known source distributions are placed within the camera and data collected. The reconstructed images are compared with the actual distribution to give a measure of the system performance. Typical distributions include point and line sources surrounded by air or water-equivalent scattering media, and phantoms where the activity is uniformly distributed in a water-equivalent medium.

The prime function of the collimators is to shield the detectors from activity outside of the cylindrical slice defined by the collimator opening. This out-of-slice activity contributes to the random and scattered coincidence rates measured by the ring and adversely affects image quality.

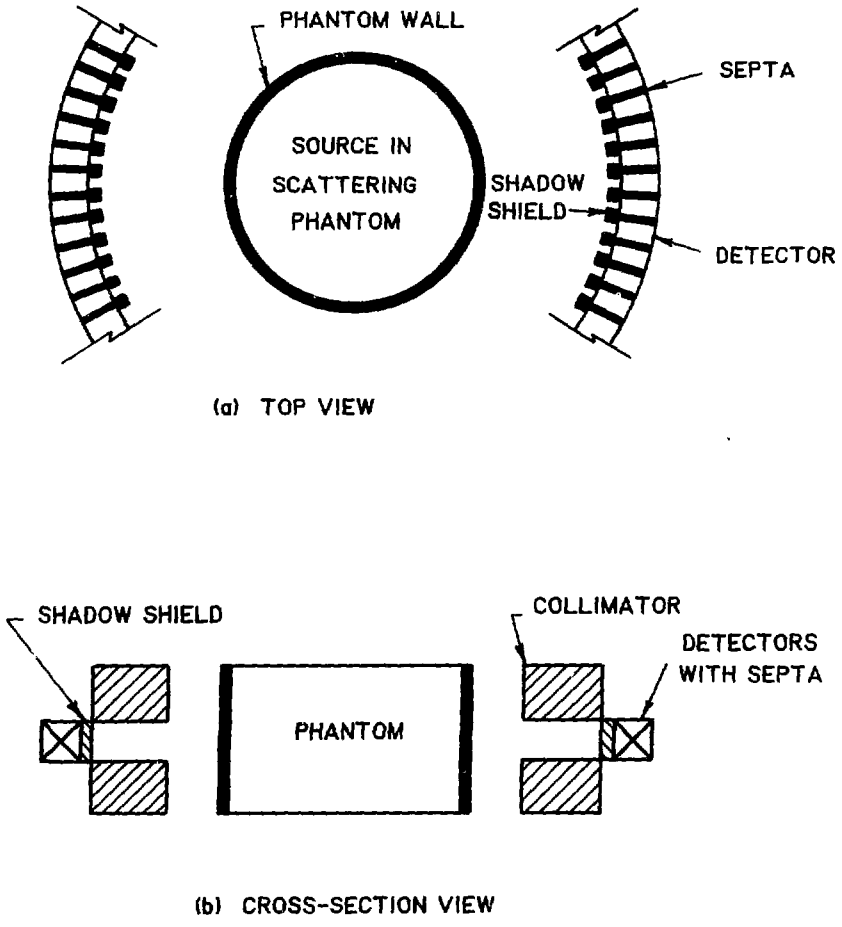

FIGURE 3: POSITRON RING CAMERA SIMULATION MODEL

The in-slice spatial resolution of a PET ring system is largely determined by the width of the detector crystal. For a fixed number of crystals, the resolution near the centre of the ring can be improved by covering part of each detector with a high-Z material, thereby reducing the effective detector width. Brooks [10] has noted that using such shadow shields can lead to degradation in the resolution at non-central points in the image. In addition, there is a reduction in the system sensitivity, the magnitude being dependent on the amount of crystal face area covered by the shadow shields.

At the present time, most positron cameras are constructed using bismuth germanate (BGO) or CsF scintillation detectors. These compounds are used, in preference to NaI(Tℓ), because of their respectively higher detection efficiency for 511 keV γ-rays, and better timing characteristics. In some systems, septa are placed between the detectors to reduce the inter-crystal transmission and scatter of γ-rays. These septa are usually made from a high-Z compound such as tungsten.

2.2 Programs

The simulation of the camera system has been divided into 5 separate programs, one for modelling the photon transport in each component (PHANTOM, COLLIMATOR, SHADOW SHIELD and DETECTOR) and a general analysis program (ANAL1). The running order for the programs is shown in Figure 4. Each program can run independently of the others, with data being transferred between each using disk files. ANAL1 is used to analyze and print out the data generated by the photon transport programs. This allows intermediate values of various system parameters to be observed.

Common to the four transport programs is a routine called MONTE which is used to track photons through the

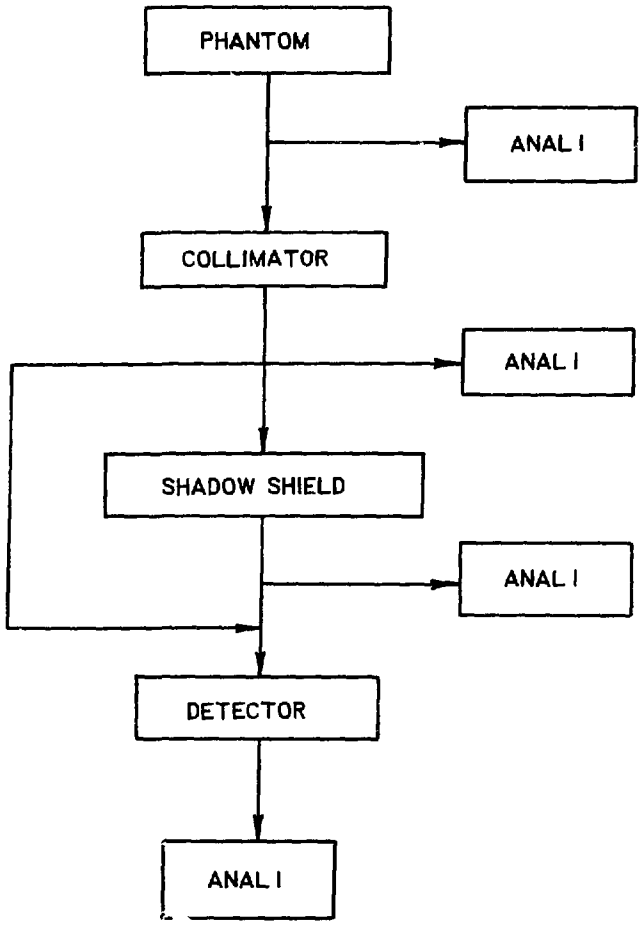

FIGURE 4: PROGRAM ORDER FLOW-CHART FOR THE POSITRON CAMERA SIMULATION

various system materials. Monte Carlo techniques are used to generate flight paths by sampling the Compton scatter and photoelectric absorption cross sections. The γ-ray tracking routine within MONTE was assembled by lifting modules from the KENO neutron tracking code [11] and modifying the appropriate sections to handle photon interactions and a 100 group energy structure (described in Appendix A). The routines carried over from KENO include:

KENO - main program used to perform general particle tracking and subroutine linkage

CROSS - subroutine used to determine region boundary crossing points for a system of nested spheres, cylinders, and/or boxes

KENOG - subroutine used to read in, test and store the region geometry description

AZIRN - subroutine used to generate the sine and cosine of a uniformly distributed azimuthal scattering angle

GTISO - subroutine used to generate direction cosines for an isotropic unit vector.

Also common to the four component programs is a data file containing a 100 x 100 matrix of equal-probability Compton-scatter cosines described in Appendix A, and 100 total Compton cross-section values at each of 100 mid-group energies.

A detailed description of each program, including input and output information, is presented in the following sections.

2.2.1 PHANTOM

PHANTOM simulates the photon transport in the source-filled phantom and the surrounding regions out to the inner

boundary of the collimator. This includes generating the annihilation locations and tracking the photons. Up to 16 regions of nested spheres, cylinders and boxes can be used to model the scattering material within the phantom, the phantom walls (if different), and the air space surrounding the phantom. Normally only 2 or 3 regions are used. A simplified flow-chart for the program is shown in Figure 5.

The input data required by PHANTOM are:

1) Equal-probability Compton-scatter cosines and total cross-section values (see Appendix A).
2) Geometry description for each region.
3) Electron density values, in electrons.barn^{-1}.cm^{-1}, for each region*.
4) Coefficients for the functional fit to the photoelectric cross section for each region (see Appendix B).
5) Cut-off value for the lower energy discriminator.
6) Maximum CPU time that the program is allowed to run.

The source generation subroutine, SOURCE, is compiled and loaded for each run. In SOURCE, the annihilation position for the positron is selected randomly within the constraints of the source geometry programmed. For example, the algorithm illustrated in Figure 6 generates a uniform activity cylindrical flood phantom. Positron range effects have not been included in the simulation, so the annihilation location also represents the positron origin. The annihilation γ-rays are assumed to be colinear. Using an isotropic distribution, the initial direction of one of the pair is chosen randomly (by subroutine GTISO) and the opposite direction is assigned to the second member of the pair.

Tracking of the individual γ-rays involves several steps. First, the mid-group energy closest to that of the photon is used to obtain the total macroscopic cross

*1 barn = $10^{-28}m^2$

section, $\sum_t$. Next the path length, λ, to the next collision point is calculated using:

$$\lambda = \frac{-1}{\sum_t} \ln(R) \qquad (1)$$

where R is a random number uniform over [0,1].

The γ-ray is then projected to this point. The photon is then either photoelectrically absorbed or scattered depending on whether or not a random number uniform over [0,1] is less or greater than the ratio of the absorption to total cross section. If scattered, the direction and energy for the scattered photon are obtained using the procedure outlined in Appendix A. This involves sampling the equal-probability groups for the scatter-angle, and generating an azimuthal angle (by subroutine AZIRN). With the new energy and direction, the procedure repeats itself until either the γ-ray energy drops below a lower energy discriminator threshold (usually 250 keV) and hence is rejected, or it reaches a boundary between two materials. Upon reaching a boundary, say between the phantom scattering material (water) and the phantom wall (aluminum), the procedure starts over again but this time using the cross sections appropriate to the new material.

When the photon reaches the radius at which the collimator begins, the tracking stops and checks are performed to see if the photon is to be stored. If the Z-axis coordinate of the photon lies between $\pm$2.5 cm, it is accepted; if the Z-axis coordinate of the photon lies outside the above limits but between $\pm$3.5 cm and it is travelling towards the x-y plane, it is accepted; otherwise it is rejected. These two criteria cover all conceivable collimator apertures and allow for edge effects due to the greyness of collimator materials at these photon energies.

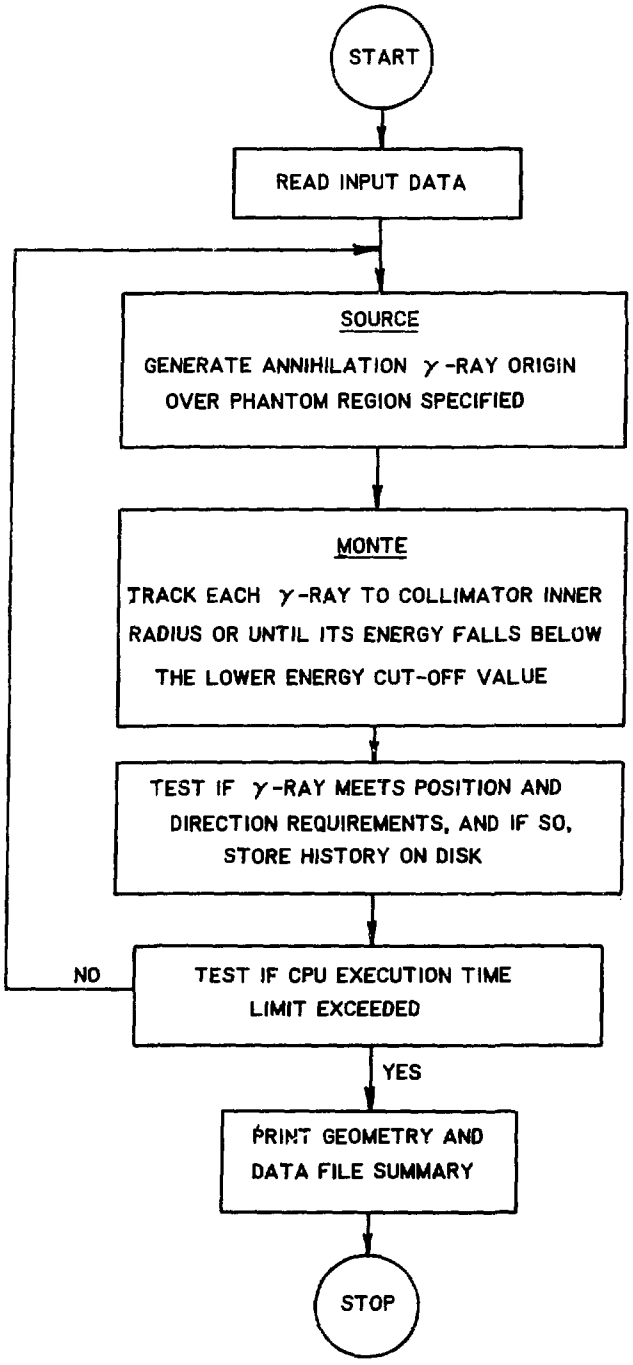

FIGURE 5: SIMPLIFIED FLOW-CHART FOR PHANTOM

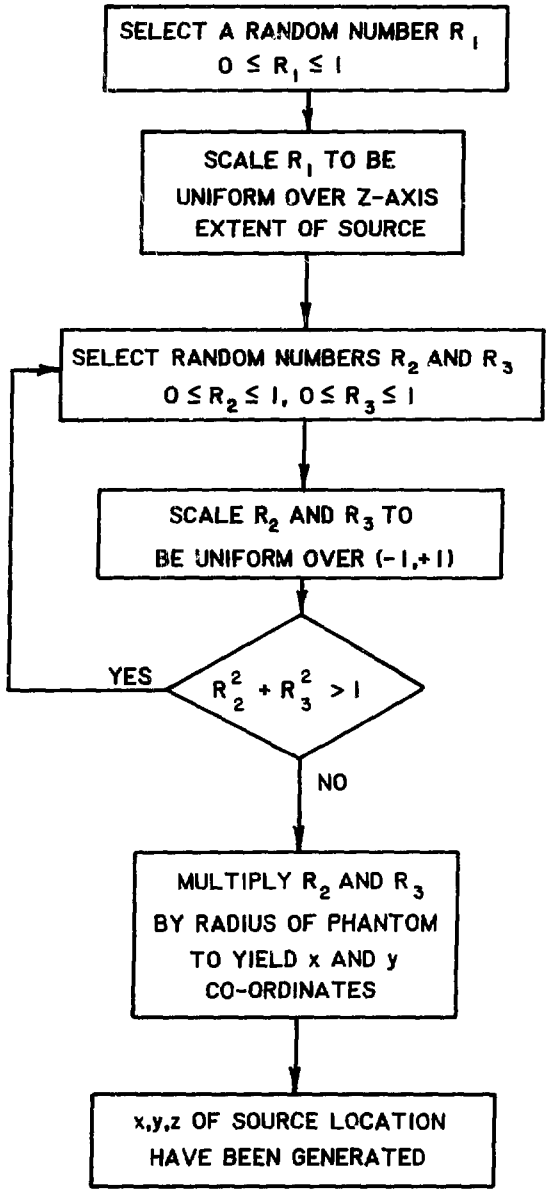

FIGURE 6: MONTE CARLO PROCEDURE TO GENERATE A POSITRON ANNIHILATION LOCATION WITHIN A UNIFORM FLOOD REGION

Both γ-rays from an annihilation are tracked until they have reached the collimator boundary and are accepted, or are rejected. If either photon is accepted, the following information is stored in the disk file:

E - photon energy at the collimator boundary
X,Y,Z - coordinate of the photon at the collimator boundary
U,V,W - direction cosines for the photon at X,Y,Z
ISR - number of scatters that the photon has undergone
X_o, Y_o, Z_o - annihilation origin of the photon
FLAG - a flag to indicate whether only one or both photons of the pair has been accepted.

To reduce the length (in bits) of the data stored on disk, an encoding/decoding scheme is implemented. Without encoding, each of the above variables would be stored as a 60 bit word from the CDC Cyber 175 computer on which the simulations are run. It was realized that this precision is not required, and hence each variable is encoded into a one to five digit positive integer number. In this way, up to five variables can be compressed into one 60 bit word, thereby saving disk space. This data compression is used in all the data transfers via disk between the five programs. As a result, one can occasionally see some quantization noise in the final data, but its level is within acceptable limits.

It was found that most of the photons passing the acceptance criteria at the collimator boundary were singles, i.e. only one of the two annihilation photons was accepted. By randomly rejecting 9 out of every 10 singles at the collimator boundary (i.e. only store 1 in 10), one is able to reduce the amount of data stored and still obtain a statistically significant number of singles.

The amount of data generated by PHANTOM is controlled by the CPU run-time specified as an input variable. Typical runs require 4000 s on a CDC CYBER 175 to generate nine million annihilations and track them through a 20 cm diameter by 12 cm tall water-equivalent flood phantom, its aluminum wall, and the surrounding air out to the collimator boundary. For this number of annihilations, about 120,000 photon histories are written to disk.

The final printout from PHANTOM contains a summary of the geometry description, the number of annihilations generated and the number of blocks of data, containing 500 photon histories each, stored on disk.

2.2.2 COLLIMATOR

COLLIMATOR models the photon transport within the collimator from its inner to outer radial boundaries. Figure 7 shows a simplified flow-chart for the program. Input data required are:

1) Equal-probability Compton-scatter cosines and total cross-section values.
2) Geometry description for each region in the collimator.
3) Electron density values, in electrons$\cdot barn^{-1} \cdot cm^{-1}$, for each region.
4) Coefficients for the functional fit to the photoelectric cross section for each region.
5) Cut-off value for the lower energy discriminator.
6) Number of data blocks of photon histories to be read.

The photons are tracked until they are absorbed, fall below the lower energy threshold, or reach the outer radius of the collimator. For those reaching the outer collimator radius, data are accepted and written to disk if the Z-axis coordinate of the photon falls within $\pm$2.0 cm. This Z-axis limit covers all conceivable detector heights.

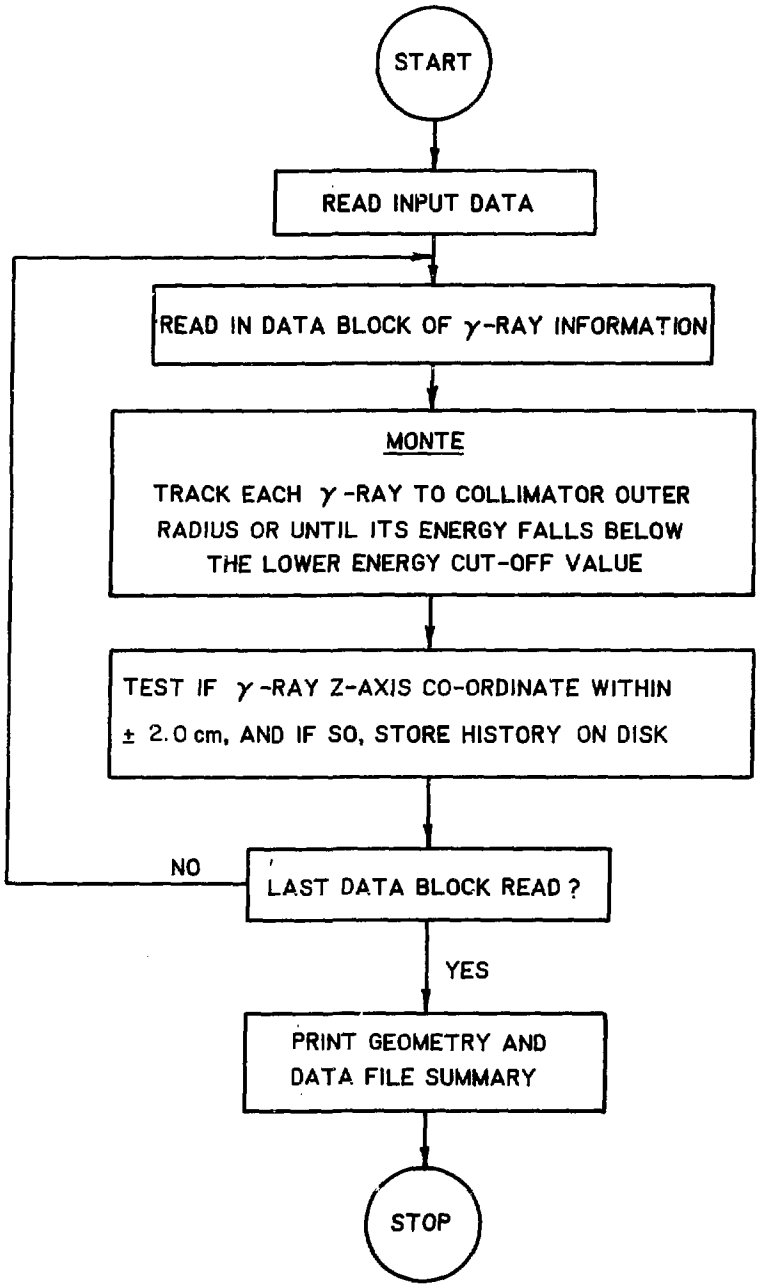

FIGURE 7: SIMPLIFIED FLOW-CHART FOR COLLIMATOR

Should only one of an initial pair of coincident photons meet the acceptance criteria, the variable FLAG for this particular photon is changed to indicate that it is now a single resulting from an interaction in the collimator. ISR (record of number of scatters that a photon has undergone) is incremented if the photon Compton scatters within the collimator and passes the acceptance criteria.

The printout contains a summary of the collimator geometry and the number of blocks of data stored.

2.2.3 SHADOW SHIELD

The shadow shield program, SHADOW SHIELD, models the γ-ray transport within the shadow shields. In the program, MONTE has been extended to model the shadow shields as sectors of an annulus (see Figure 3). A simplified flowchart for the program is shown in Figure 8. The input data required by SHADOW SHIELD are:

1) Equal-probability Compton-scatter cosines and total cross-section values.
2) Geometry description for the shadow shield annulus (number of shields and their height, depth, and width).
3) Electron density value, in electrons$\cdot$barn$^{-1}\cdot$cm^{-1} for the shadow shield material.
4) Coefficients for the functional fit to the photoelectric cross section for the shadow shield material.
5) Cut-off value for the lower energy discriminator.
6) Number of data blocks of photon histories to be read.

With the input geometry information, the program determines where each shield is located in angular position about the ring and assumes that the remaining space in the annulus is air.

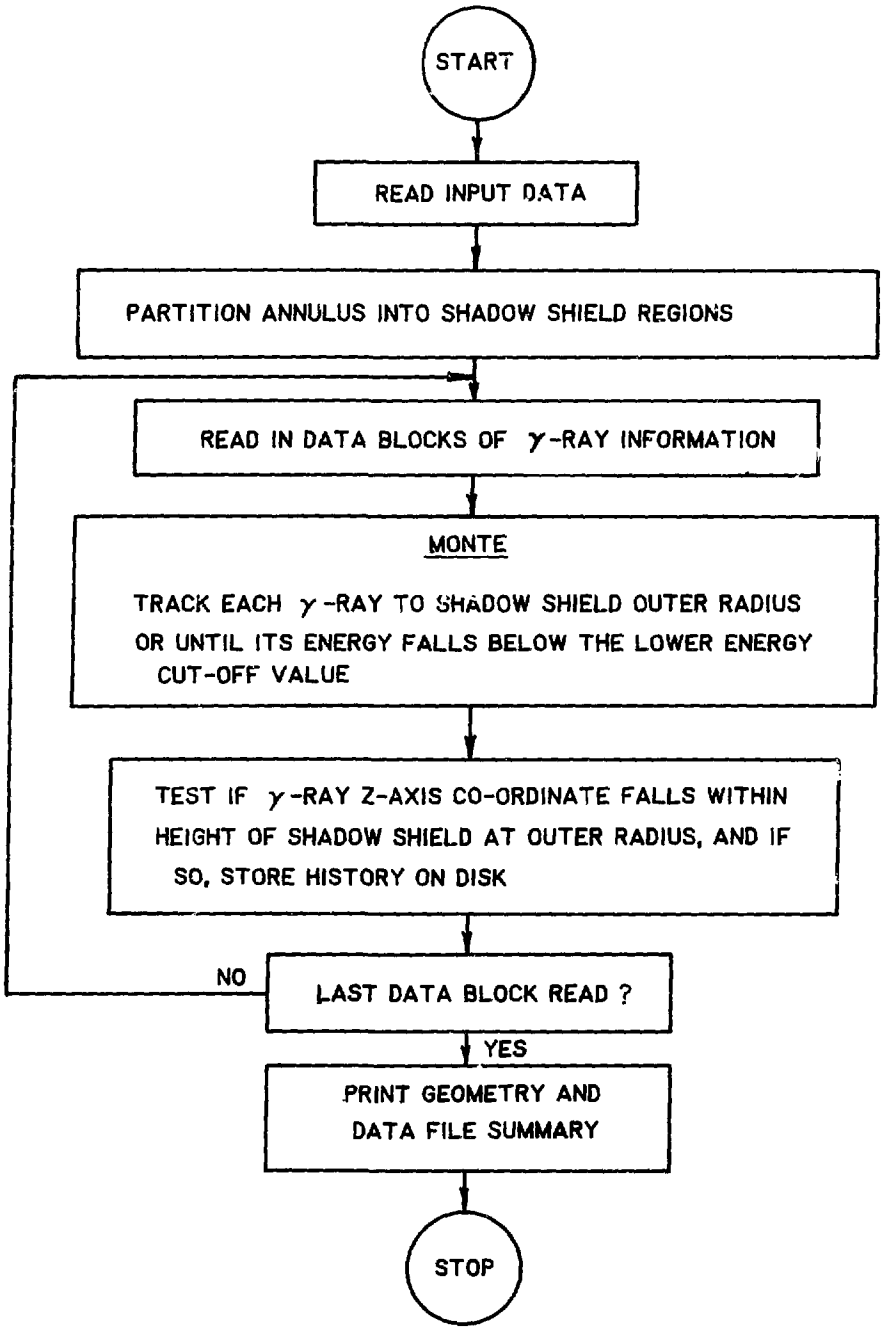

FIGURE 8: SIMPLIFIED FLOW-CHART FOR SHADOW SHIELD

The photons are tracked until they are photoelectrically absorbed, fall below the lower energy threshold, or reach the system boundaries. Data are accepted and written to disk if the Z-axis coordinate of the photon falls within the height of the shadow shield at the back face. As in COLLIMATOR, should only one of a pair of coincident photons meet the acceptance criteria, the variable FLAG for this particular photon is changed to indicate that it is now a single event. ISR is also incremented if the photon scatters and is accepted.

The printout contains a summary of the geometry parameters and the data file information.

2.2.4 DETECTOR

The detector simulation program, DETECTOR, models a ring of up to 244 detectors with inter-crystal tungsten alloy (Kennertium) septa. As in SHADOW SHIELD, MONTE has been extended to handle the detectors and septa as sectors of an annulus. A simplified flow-chart for the program is shown in Figure 9. Input data include:

1) Equal-probability Compton-scatter cosines and total cross-section values.
2) Geometry description for the detector ring annulus. The following information is required: detector height, detector depth, septa width at the ring face, and the number of detectors.
3) Electron density value, in electrons $\cdot barn^{-1} \cdot cm^{-1}$ for the detector material. The Kennertium values are programmed into the code.
4) Coefficients for the functional fit to the photoelectric cross section for the detector material.
5) Cut-off value for the lower energy discriminator.

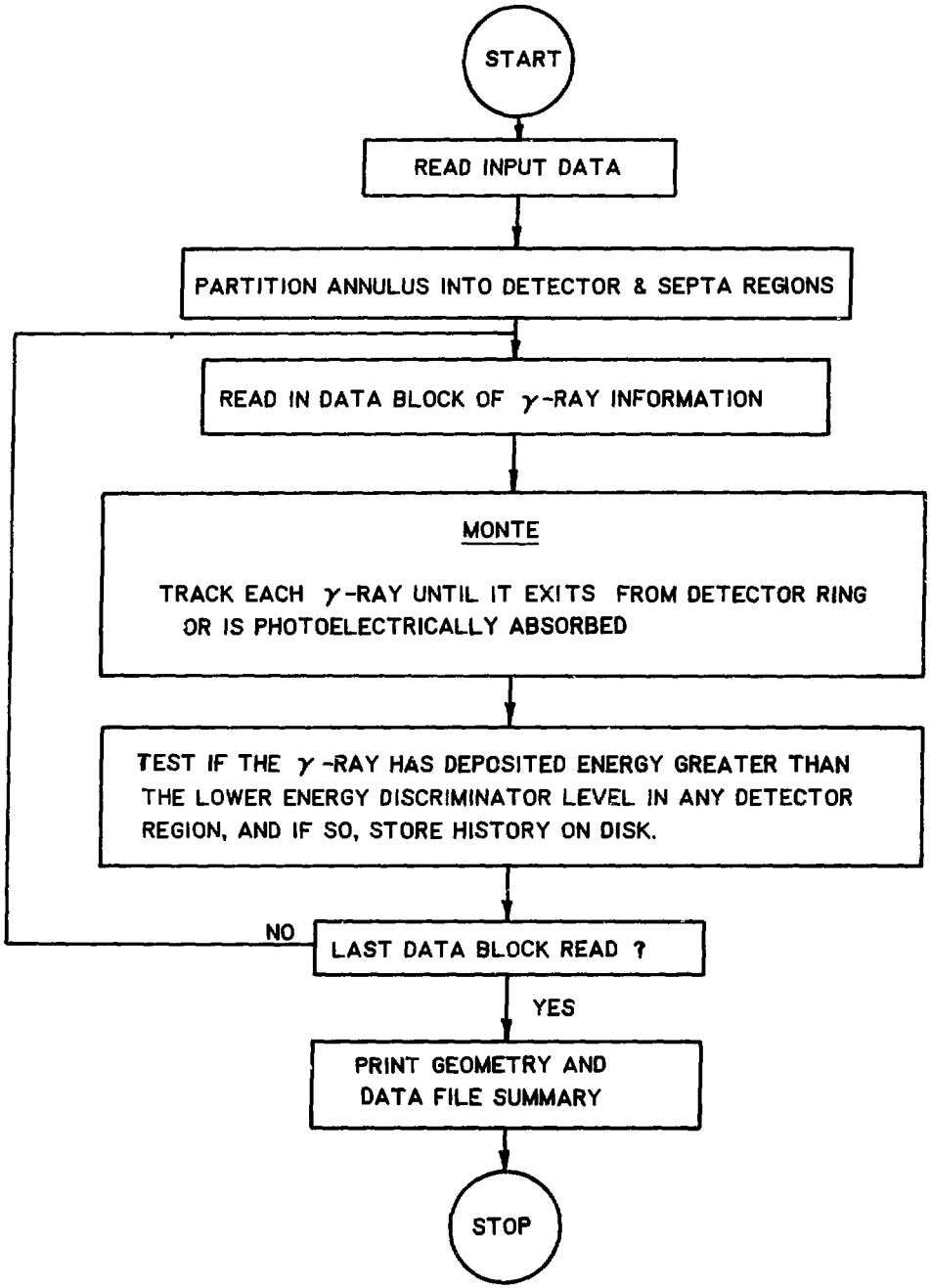

FIGURE 9: SIMPLIFIED FLOW-CHART FOR DETECTOR

6) Number of data blocks of photon histories to be read.

The ring is divided into alternating sectors of septa and detector material with the septa being centred at the mid-point of the shadow shields.

In DETECTOR, photons are tracked until they escape from the detector ring or are photoelectrically absorbed. A photon is considered to be detected if it deposits more than a given amount of energy (usually 250 keV) in a single detector. The energy deposition is tabulated by recording the amount of energy deposited in a given detector or septa region following an interaction. When the photon tracking is terminated, the energy deposited in each detector is compared with the lower energy threshold value. The first detector in which the total energy deposited exceeds this limit is considered to have detected the photon. The final X,Y,Z coordinates for the detected photons are assigned to be those of the centre of the face of the detector in which it is registered. Detection is the sole acceptance criteria for a photon history to be written to disk.

ISR is not incremented by DETECTOR since inter-crystal scatter and penetration is assumed to be a resolution problem, separate from scattering within the phantom, collimator or shadow shields. FLAG is, however, changed should a coincident photon not have its mate detected.

In addition to the geometry and data file summary provided in the final printout, a tabulation of the photons in the following classifications is provided for the true coincidence and scattered coincidence data and the single events:

Detected - those that enter a detector and deposit more energy than the lower energy threshold in that detector;

Moved - those that enter a detector or septa region but deposit more energy than the lower energy threshold in another detector region;

Lost - those that fail to be detected.

2.2.5 ANAL1

ANAL1 has two modes of operation. In the normal mode, the program is used as an analysis routine. It provides a summary of ring performance parameters calculated from the photon histories read from a disk file written by any of the four photon-transport programs. In the survey mode, ANAL1 is used to model the effects that different collimators have on the performance parameters assuming that they are black absorbers. In this case, the PHANTOM output disk file is read and the photons are projected to the detector ring radius. In the survey mode, the analysis assumes the following: the collimators are ideal absorbers (i.e. optical collimators), the detectors are 100% efficient, the collimator gap is a vacuum, and at the detector ring, photons are detected if they hit the detector face and their energy is within the discriminator level thresholds.

A flow-chart for ANAL1 is shown in Figure 10. To simplify the coding, the ideal collimator is always included as part of the calculation. The normal mode of operation is obtained by specifying a collimator length of zero in the input. Input data required by the program include:

1) Collimator dimensions (length and height of opening).
2) Height of detectors.
3) Axial extent of source and scattering medium in phantom.
4) Values for the upper and lower energy discriminators.
5) Fractional energy resolution, i.e. the full width at half maximum (FWHM) of the assumed Gaussian distribution (see Appendix C).

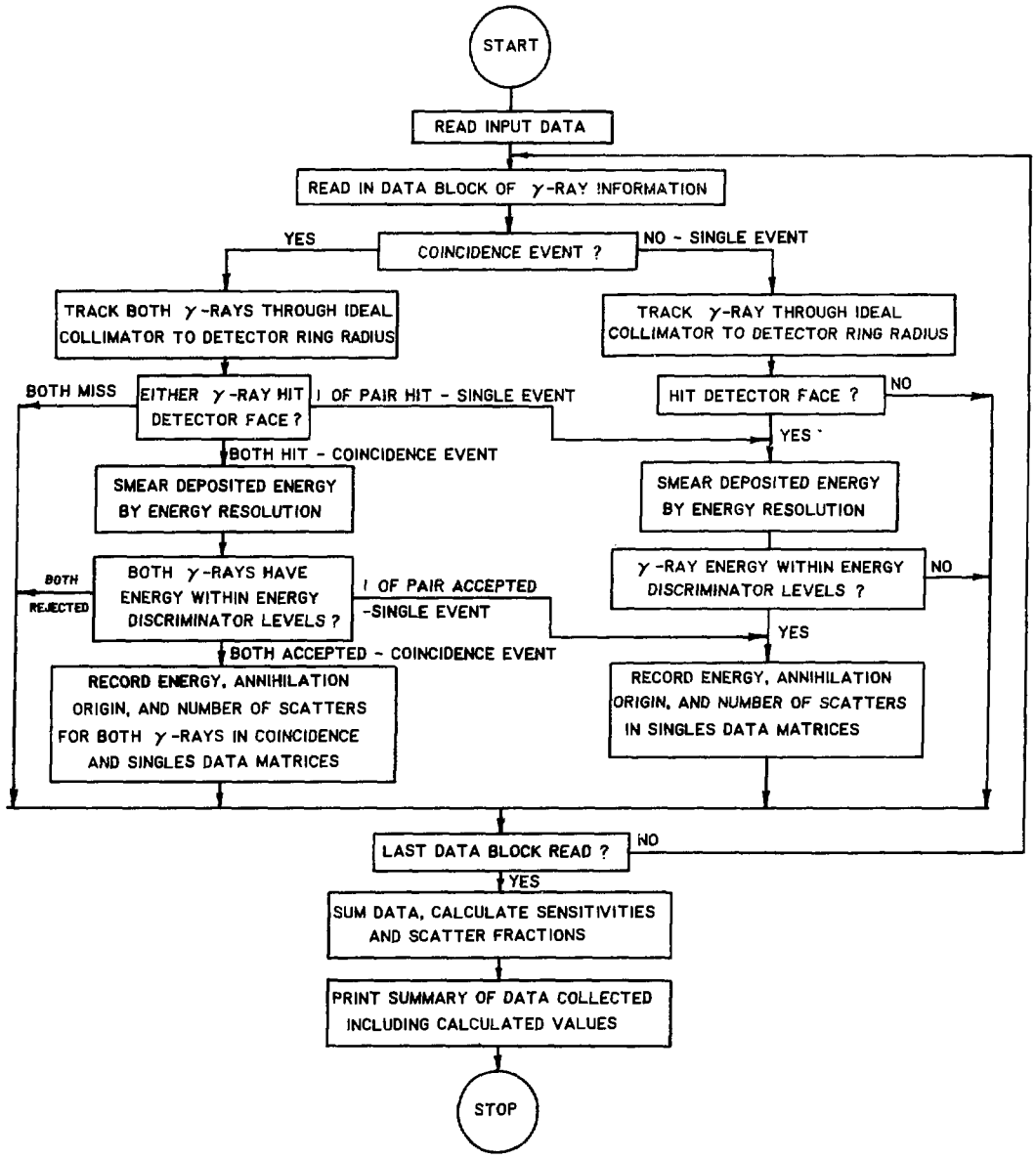

FIGURE 10: SIMPLIFIED FLOW-CHART FOR ANAL I

6) Number of photon pairs generated in the phantom.
7) Number of data blocks to be read from the disk file.
8) Control parameters for printing the final output.

Photons are considered to be detected if their deposited energy, after the inclusion of energy resolution effects (see Appendix C), is within the energy discrimination levels specified.

In ANAL1, the photons are sorted into two major classifications: coincident or single. Within each classification, subsorting is based on pertinent details for each photon, such as its energy, position, annihilation z-axis origin, and number of scatters it underwent in the phantom, collimator or shadow shields. These details are used to obtain information not normally available from experimental data. Upon reading all the photon data from the input file, the matrices into which the information has been sorted are adjusted and summed to yield the desired output data. Included in this data are ratios such as scatter fraction, in-plane to out-of-plane coincidence and singles fractions, and system efficiencies (defined below). In addition, a subset of the data matrices are printed out depending upon the printing control parameters chosen. The primary ring parameters that are calculated in ANAL1 and that are contained in the output, along with some of the matrices that are also available for output, are listed below.

Absolute Coincidence Efficiency - the fraction of annihilations that contributed to either true or total (true + scatter) coincidence events. A true coincidence event is one in which neither γ-ray was Compton scattered by the time it reached the detector face. On the other hand, a scattered

coincidence event is one where one or both of the γ-rays were scattered in the phantom, collimator, or shadow shields before detection.

Coincidence Sensitivity - the sensitivity of a PET ring system is defined as the number of coincidence events (true or total) detected per $\mu Ci/cm^3$* of activity uniformly dispersed in a flood phantom. Though no activity level is specified in the input data, one can derive this value using the number of detected coincidences and the number of annihilations in the phantom.

Coincidence Fractions - fraction of coincidence events that were either trues or scatters. These are further subdivided into those whose annihilation position was in-plane (as defined by the collimator aperture or opening) or out-of-plane (annihilation origin outside the Z-axis extent of the collimator opening).

Slice Coincidence Scatter Fraction - fraction of scattered coincidence events whose annihilation origin was either in-plane or out-of-plane.

Absolute Singles Efficiency - ratio of photons detected to total number generated.

Singles Fraction - fraction of photons detected whose annihilation origin was either in-plane or out-of-plane.

Energy Spectra - the energy spectra of the detected photons

---

* 1 μCi = 37 kBq

are recorded in 20 keV bins as a function of the type of event (coincident or single) and the number of scatters.

Coincident Scatter Matrices - four-by-four matrices that record the number of coincident events as a function of the number of scatters for each photon and as a function of the annihilation origin (in-plane and out-of-plane).

Mean Projection Data - a projection is a profile through the object as sampled by parallel coincidence detector pairs. The mean projection represents the sum of all possible projections. It is useful for circularly symmetric objects where the statistics can be improved.

Z-axis Position Data - line vectors that record the Z-axis annihilation origin position for singles, true coincidence, scattered coincidence and total coincidence events. The data are recorded in 1 mm steps from -10.0 cm to +10.0 cm. This data is used to judge the effectiveness of various collimator and detector shapes in rejecting out-of-plane singles and scattered coincidence events.

3. SUMMARY

A Monte Carlo simulation of a single-ring positron emission tomography camera has been described. By using standard techniques, the photon transport within phantoms, collimators, shadow-shields and detectors has been successfully modelled. The simulation routines are sufficiently general to be able to model most camera geometries and materials.

This package has been used to predict the coincidence and axial response of several existing and proposed ring cameras. In addition, the simulation can be used as a design aid to study the effects that each component has on the over-all system response. These studies are in progress and the results will be published when completed.

4. REFERENCES

[1] T.F. Budinger and G.T. Gullberg, "Three Dimensional Reconstruction in Nuclear Medicine Emission Imaging", IEEE Trans. Nucl. Sci. NS-21, 1974, p. 2.

[2] S.E. Derenzo, H. Zaklad and T.F. Budinger, "Analytical Study of a High-Resolution Positron Ring Detector System for Transaxial Reconstruction Tomography", J. Nucl. Med. 16(12), 1975, p. 1166.

[3] S.E. Derenzo, "Method of Optimizing Side Shielding in Positron-Emission Tomographs and for Comparing Detector Materials", J. Nucl. Med. 21(10), 1980, p. 971.

[4] L.R. Carroll, G.O. Hendry and J.D. Currin, "Design Criteria for Multi-Slice Positron Emission-Computed Tomography Detector Systems", IEEE Trans. Nucl. Sci. NS-27(1), 1980, p. 485.

[5] L. Eriksson and Ż.H. Cho, "Efficiency Optimization Analysis for Dynamic Function Studies with 3-D Transaxial Positron Cameras", Comput. Biol. Med. 6, 1976, p. 361.

[6] E.J. Hoffman, M.E. Phelps, N.A. Mullani, C.S. Higgins and M.M. Ter-Pogossian, "Design and Performance Characteristics of a Whole-Body Positron Transaxial Tomograph", J. Nucl. Med. 17(6), 1976, p. 493.

[7] E.J. Hoffman and M.E. Phelps, "An Analysis of Some of the Physical Aspects of Positr.. Transaxial Tomography", Comput. Biol. Med. 6, 1976, p. 345.

[8] R.A. Brooks, V.J. Sank, G. Di Chiro, W.S. Friauf and S.B. Leighton, "Design of a High Resolution Positron Emission Tomograph: The Neuro-PET", J. Comput. Assist. Tomogr. 4(1), 1980, pg. 5.

[9] E.D. Cashwell and C.J. Everett, "A Practical Manual on the Monte Carlo Method for Random Walk Problems", Pergamon Press, London (1959).

[10] R.A. Brooks, V.J. Sank, W.S. Friauf, S.B. Leighton, H.E. Cascio and G. DiChiro, "Design Consideration for Positron Emission Tomography", IEEE Trans. Biomedical Engineering BME-28 (2), 1981, p. 158.

[11] G.E. Whitesides and N.F. Cross, "KENO-A Multigroup Monte Carlo Criticality Program", CTC-5, Oak Ridge National Laboratory (1969).

[12] C.M. Davisson, "Interaction of γ-Radiation with Matter" and "γ-ray Absorption Coefficients" in "Alpha-, Beta-, and Gamma-Ray Spectroscopy", Vol. 2, K. Siegbahn, Ed., North-Holland Publishing Co., Amsterdam (1965).

APPENDIX A

SIMULATION OF COMPTON SCATTER

A.1 General

This appendix outlines the implementation of a Monte Carlo procedure to simulate Compton scattering.

A.2 Selection of Probability Groups for Scatter

Figure A.1 shows a hypothetical energy spectrum for 511 keV γ-rays following a number of scatters in water. The probability, $P(E \rightarrow E')$, that a γ-ray will scatter from energy interval ΔE at energy E to energy interval $\Delta E'$ at energy E' is given by:

$$P(E \rightarrow E') = \frac{\int_{\Delta E} \phi(E)\,dE \int_{\Delta E'} \sigma_s(E \rightarrow E')\,dE'}{\int_{\Delta E} \phi(E)\sigma_s(E)\,dE} \qquad (A.1)$$

where $\phi(E)$ is the energy spectrum for the γ-rays
$\sigma_s(E)$ is the total cross section for scatter
$\sigma_s(E \rightarrow E')$ is the differential scatter cross section from energy E to E'.

For a large energy interval ΔE, the correct selection of an analytical form for $\phi(E)$ is important when the cross-sections vary rapidly with energy. As ΔE decreases, the variation in $\phi(E)$ over the interval decreases, until at some point it can be assumed that $\phi(E)$ is a constant over the interval. In this case, equation (A.1) becomes:

$$P(E \rightarrow E') \quad \frac{\int_{\Delta E} dE \int_{\Delta E'} \sigma_s(E \rightarrow E')\,dE'}{\int_{\Delta E} \sigma_s(E)\,dE} \qquad (A.2)$$

which can be evaluated from the known cross-sections.

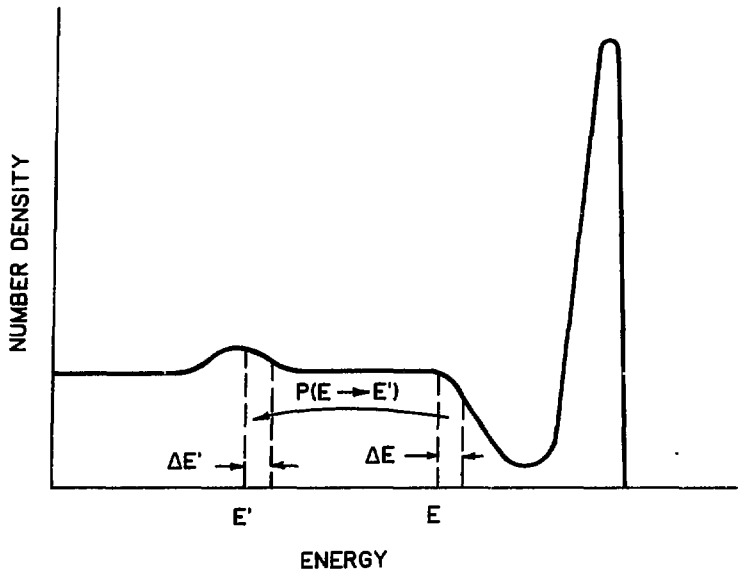

FIGURE A.1: HYPOTHETICAL γ-RAY ENERGY SPECTRUM FOLLOWING A NUMBER OF SCATTERS IN WATER. P(E→E') IS THE PROBABILITY THAT THE γ-RAY WILL SCATTER FROM ENERGY INTERVAL ΔE AT ENERGY E TO ENERGY INTERVAL $\Delta E'$ AT ENERGY E'.

The Monte Carlo approach to sampling a probability distribution involves selecting a random number, R, uniform on the range 0 through 1, and then integrating the normalized probability distribution P(v) so that the integral equals the random number. That is, the variable x is given by:

$$R = \frac{\int_{x_{min}}^{x} P(v)dv}{\int_{x_{min}}^{x_{max}} P(v)dv} \qquad (A.3)$$

where x_{min} and x_{max} are the minimum and maximum values that can be obtained.

The value of x satisfying equation A.3 is the new parameter used subsequently in the calculation. In practice in Monte Carlo calculations, the probability function is divided up into groups and the integral is replaced by summation. In the example cited above, the energy spectra would be divided into groups and $P(E \rightarrow E')$ is replaced by $P(m \rightarrow i)$, the probability of scatter from group m to i (see Figure A.2). In particular, to determine the energy group into which a γ-ray scatters, the Monte Carlo procedure illustrated in Figure A.3 could be used. However, for a large number of groups, this procedure is time-consuming and thus should be avoided if possible.

In the discussion thus far, the exact energy group structure for the γ-rays has been ignored. Suppose that the structure had been selected so that for one particular group m, the probability of scatter into all the other groups in an n-group structure is equal, that is:

$$P(m \rightarrow i) = \frac{1}{n} \quad \text{for all } i \qquad (A.4)$$

In the case of this one group, the Monte Carlo procedure to find the new group, upon scatter, is reduced to that shown in Figure A.4. This algorithm is obviously faster than

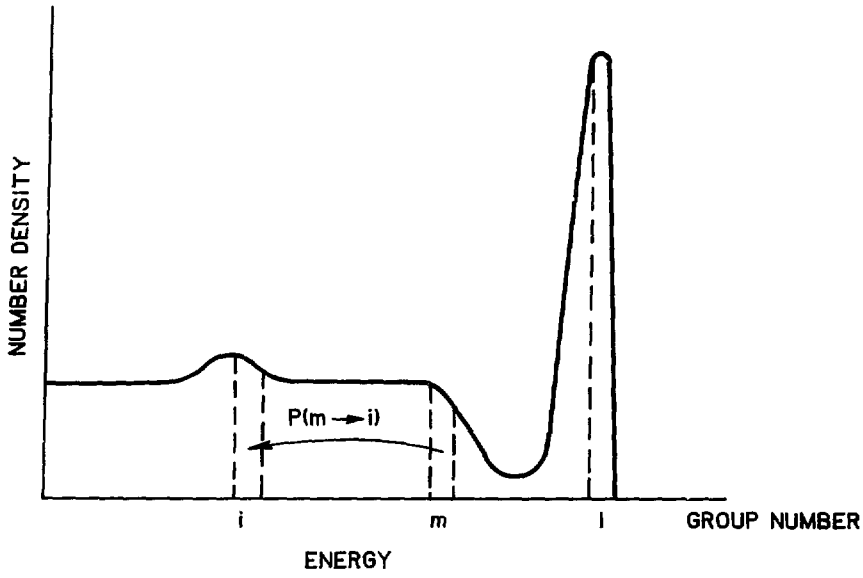

FIGURE A.2: HYPOTHETICAL γ-RAY ENERGY SPECTRUM FOLLOWING A NUMBER OF SCATTERS IN WATER. SPECTRUM OF FIGURE A.1 HAS BEEN QUANTIZED INTO GROUPS AND P(E → E') HAS BEEN REPLACED BY P(m → i).

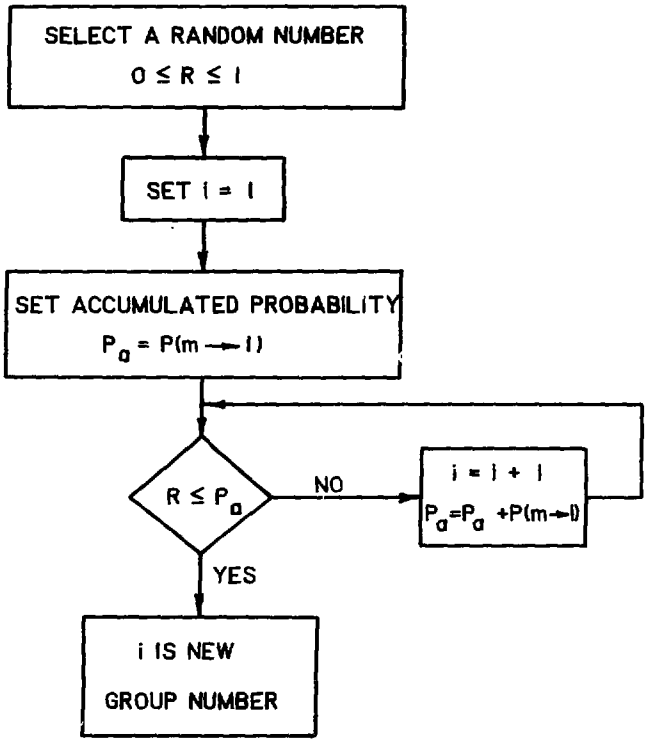

FIGURE A.3: MONTE CARLO PROCEDURE TO DETERMINE A NEW ENERGY GROUP.

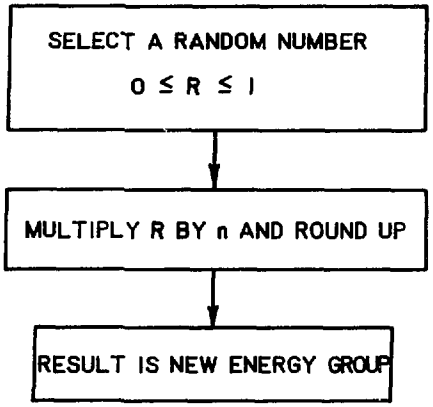

FIGURE A.4: SIMPLIFIED MONTE CARLO PROCEDURE TO DETERMINE A NEW ENERGY GROUP WHEN ALL $P(m \rightarrow i)$ ARE EQUAL.

that of Figure A.3. It will now be intuitively shown that, for an energy group structure in which the group energy width is sufficiently narrow such that the cross-section can be considered to be constant over each group, this procedure can be applied to all energy groups.

Suppose that one were to start with some predetermined n-group energy structure for the γ-rays. Then for each of these energy groups, a new n-group structure can presumably be found such that the probability for scatter into each of the new groups is equal. In general, for each one of the initial n-groups, one would have a different set of equal-probability energy groups for the scattered γ-rays. Thus after a single scatter one would require n separate n-group energy structures to keep track of the scattered γ-rays. A second scatter would require n^2 n-group structures, and so on. This situation is clearly impossible to handle computationally and hence an equal-probability group structure for the scattered γ-rays is only viable if we can transfer the γ-ray back into one of the initial energy groups after a scatter has taken place. Thus the procedure used is as follows: the initial energy spectrum is divided into n groups, and for each of these groups, an equal-probability n-group scatter structure is determined. After a single scatter, the new energy of the γ-ray is calculated and this energy will fall within the energy limits for one of the initial groups used for the γ-ray prior to scatter. For a large number of initial groups, the cross section over each of the groups can be considered to be constant, and thus the γ-ray can be assigned to this new group. The equal-probability structure already available for this group can be used to determine the result for the next scatter. In this way, a method of coupling a predetermined energy group structure to an equal-probability scatter formalism is found.

A.3 Compton Scattering

As illustrated in Figure A.5, an incident γ-ray can be scattered by an atomic electron, resulting in a transfer of momentum and energy to the electron. The scattered γ-ray is emitted at an angle Θ to initial direction, and its energy is given by:

$$E' = \frac{E}{1 + \frac{E}{m_o c^2}(1-\cos\Theta)} \qquad (A.5)$$

where E' is the energy of the scattered photon
E is the initial photon energy
$m_o c^2$ is the rest-mass energy of an electron (511 keV)
Θ is the scatter angle of the photon.

The equal-probability group concept described above is used to simulate this scattering process. Referring to Figure A.6, an initial 100 energy group structure was chosen based upon a mid-group energy of 511 keV for group 1 and a uniform step size of 5 keV between mid-group energies. For each mid-group energy, the differential Compton cross section $\frac{d\sigma}{d\Theta}$, given by the Klein-Nishina formula [12], was numerically integrated in steps of 0.1° to find 100 equal-probability scatter groups.

$$\frac{d\sigma}{d\Theta} = 2\pi r_o^2 \sin\Theta \frac{(1+\cos^2\Theta)}{2} \frac{}{(1+\alpha(1-\cos\Theta))^2} \left(1 + \frac{\alpha^2(1-\cos\Theta)^2}{(1+\cos^2\Theta)(1+\alpha(1-\cos\Theta))}\right) \qquad (A.6)$$

where $\alpha = E/511$
E is the initial energy of the γ-ray before scattering (in keV)
Θ is the scatter angle
r_o is the classical electron radius ($e^2/(m_o c^2)$)
e is the elementary charge of the electron

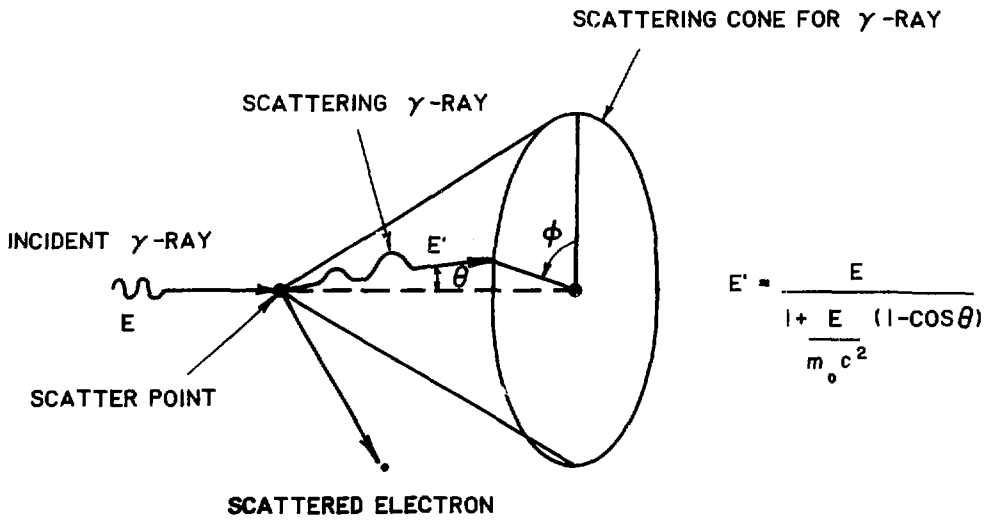

FIGURE A.5: THE COMPTON-SCATTER PROCESS

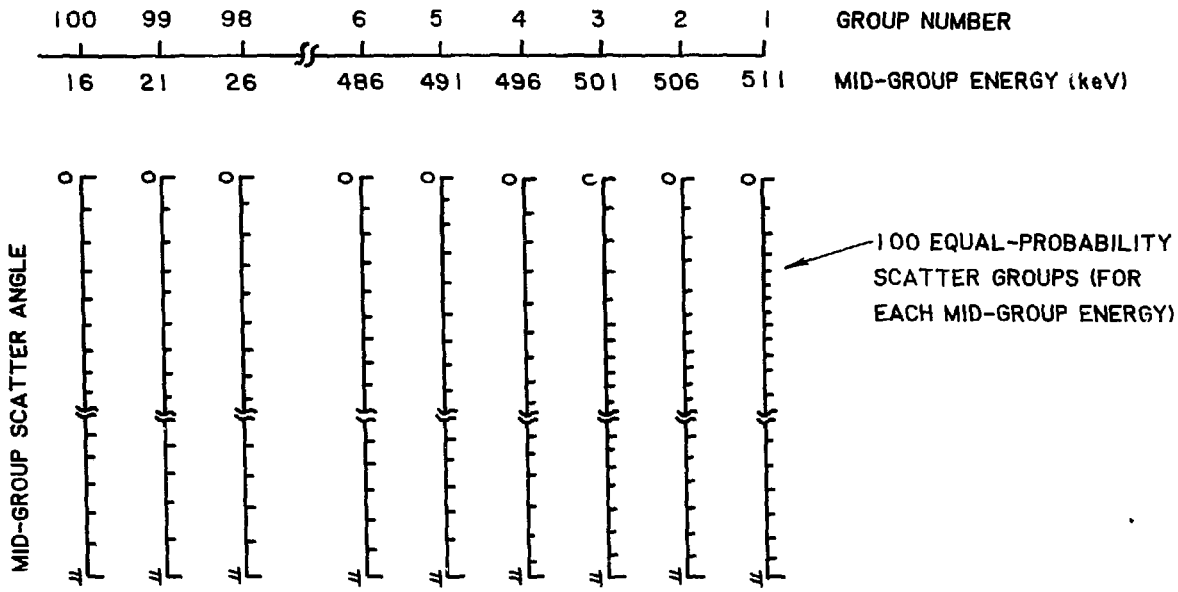

FIGURE A.6: DIAGRAM ILLUSTRATING THE APPLICATION OF AN EQUAL-PROBABILITY GROUP CONCEPT TO COMPTON SCATTER OF 511 keV γ-RAYS. THE ENERGY SPECTRUM IS DIVIDED INTO 100 ENERGY GROUPS OF 5 keV WIDTH, AND FOR EACH GROUP, 100 EQUAL-PROBABILITY SCATTER ANGLES ARE DETERMINED FROM THE DIFFERENTIAL SCATTER CROSS SECTION AT THAT ENERGY.

These groups were tabulated in terms of their scatter-angle cosines and stored on disk for use in a Monte Carlo tracking procedure. They were stored in this form, rather than in terms of the angle or energy, since the cosine is used to calculate both the new energy and the direction cosines for the scattered photon.

The total Compton-scatter cross section (σ) is given by:

$$\sigma = 2\pi r_o^2\left[\frac{1+\alpha}{\alpha^2}\left(\frac{2(1+\alpha)}{(1+2\alpha)} - \frac{\ell n(1+2\alpha)}{\alpha}\right) + \frac{\ell n(1+2\alpha)}{2\alpha} - \frac{1+3\alpha}{(1+2\alpha)^2}\right] \qquad (A.7)$$

Values for each mid-group energy were calculated and stored on disk with the equal-probability scatter cosines.

The total cross section can be obtained by numerically integrating Equation A.6 to check the differential cross-section routine. The results thus generated are shown in Figure A.7, and compared with the theoretical curve calculated from the analytical formula for the total cross section. The agreement is excellent.

To obtain the macroscopic cross section, Σ_s, for a specific material, the total Compton cross section must be multiplied by the electron density (ρ_e). The electron density values used in the simulation for various materials are shown in Table A.1.

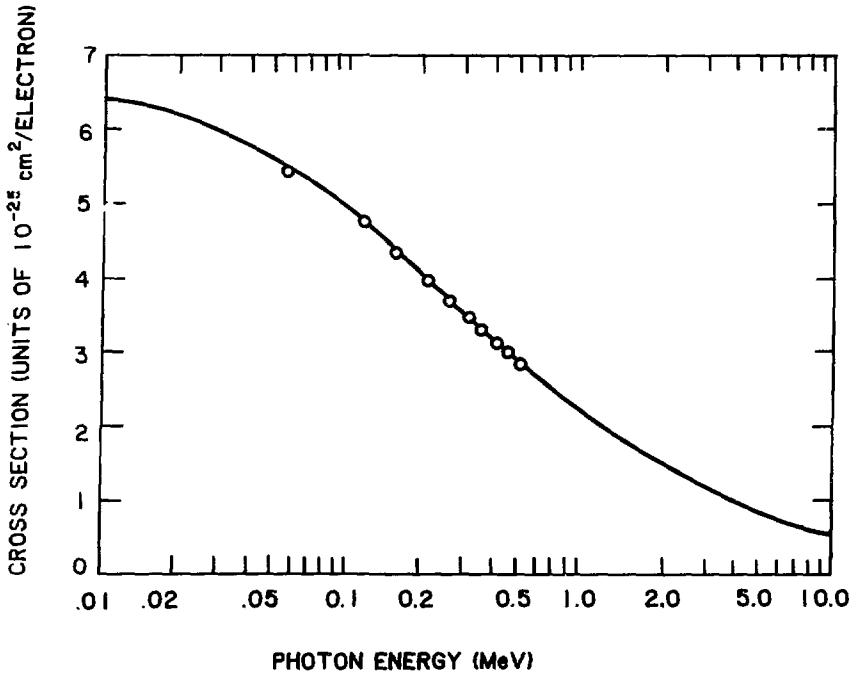

FIGURE A.7: TOTAL COMPTON CROSS SECTION VERSUS ENERGY. THE SOLID LINE IS THE THEORETICAL CURVE WHILE THE OPEN CIRCLES WERE OBTAINED BY NUMERICAL INTEGRATION OF THE KLEIN-NISHINA DIFFERENTIAL CROSS SECTION.

TABLE A.1: Electron Density Values for Various Materials

Material	Electron Density ρ_e (electrons/cm^3)
Air	1×10^{17}
Aluminum	0.78×10^{24}
BGO ($Bi_4Ge_3O_{12}$)	1.678×10^{24}
Foam	0.013×10^{24}
Lead	2.702×10^{24}
Tungsten Alloy*	3.729×10^{24}
Vacuum	0
Water	0.3335×10^{24}

*Commercially known as Kennertium or Heavymet

APPENDIX B

SIMULATION OF PHOTOELECTRIC ABSORPTION

For photon energies of the order of a few hundred keV, the dominant interaction mechanism in low Z materials is Compton scatter. With increasing Z, however, the photoelectric effect becomes more important, and at high Z, it is the dominant interaction mechanism. Photoelectric cross-section data for various materials are given in reference 12 as a function of energy. For use in the Monte Carlo simulation, these data were fit to the simple functional form:

$$\sigma_\gamma = AE^{-B} \qquad \text{(B.1)}$$

where σ_γ is the photoelectric cross section
A,B are the fitting coefficients
E is the γ-ray energy (keV).

The fitted results are compared with the tabulated data in Table B.1 for selected materials of interest. The values for the parameters A and B were obtained by trial and error so that a good fit over the range 150 to 500 keV was achieved. The increasing discrepancy between the calculated value of σ_γ and the tabulated value below 150 keV was not considered important since at these energies the photoelectric cross section is becoming effectively infinite.

TABLE B.1: Photoelectric Cross Sections for Various Materials

	Material					
	Lead		Tungsten Alloy*		BGO**	
Fit coefficient - A	1.422×10^8		1.950×10^8		1.253×10^9	
B	2.496		2.654		2.604	
	Photoelectric Cross Section (barns/molecule)***					
Photon Energy (keV)	Tabulated	Fitted	Tabulated	Fitted	Tabulated	Fitted
100	1780	1448	1000	959	8100	7762
150	596	527	326	327	2700	2700
200	275	257	148.8	152.4	1250	1277
300	93.4	93.3	50.5	52.0	421	444
400	45.7	45.5	23.8	24.2	209	210
500	26.1	26.1	13.4	13.4	123	117

* Tungsten alloy values assumed to be 80% those of pure tungsten

** BGO ($Bi_4Ge_3O_{12}$) approximated by $Pb_4Cu_3O_{12}$ due to the absence of data for Bi and Ge in the tabulation [12]

*** 1 barn = $10^{-28} m^2$

APPENDIX C

SIMULATION OF SCINTILLATOR AND PHOTOMULTIPLIER STATISTICS

Statistical processes within the scintillation crystals and photomultipliers lead to a broadening of the energy peak for detected γ-rays. To account for this, the energy deposited in the detector, obtained from the detector simulation, is broadened assuming a Gaussian distribution. This shape is programmed into the simulation by modifying the energy of the γ-ray by an amount chosen from a Gaussian distribution of random numbers with a specified FWHM corresponding to the desired energy resolution. That is:

$$E_{recorded} = E_{deposit} + \left(E_{deposit} \cdot FWHM \cdot R_G \cdot 0\ 42466\right) \quad (C.1)$$

where $E_{recorded}$ - energy of γ-ray recorded for use in the data analysis

$E_{deposit}$ - energy deposited by the γ-ray in a given detector as obtained from the Monte Carlo detector simulation

FWHM - the full width at half maximum of the Gaussian

R_G - Gaussian distributed random number (mean of 0, standard deviation of 1)

0.42466 - conversion factor between FWHM and standard deviation notation for Gaussian distribution.

ISSN 0067 - 0367

To identify individual documents in the series we have assigned an AECL- number to each.

Please refer to the AECL- number when requesting additional copies of this document

from

Scientific Document Distribution Office
Atomic Energy of Canada Limited
Chalk River, Ontario, Canada
K0J 1J0

Price $4.00 per copy

ISSN 0067 - 0367

Pour identifier les rapports individuels faisant partie de cette série nous avons assigné un numéro AECL- à chacun.

Veuillez faire mention du numéro AECL- si vous demandez d'autres exemplaires de ce rapport

au

Service de Distribution des Documents Officiels
L'Energie Atomique du Canada Limitée
Chalk River, Ontario, Canada
K0J 1J0

Prix $4.00 par exemplaire

2665–82